Neurocomputing 322 (2018) 187–194

Contents lists available at ScienceDirect

Neurocomputing

journal homepage: www.elsevier.com/locate/neucom

Delay aware transient stability assessment with synchrophasor recovery and prediction framework

James J.Q. Yu[a,*], David J. Hill[a], Albert Y.S. Lam[a,b]

[a] Department of Electrical and Electronic Engineering, The University of Hong Kong, Pokfulam, Hong Kong
[b] Fano Labs, Shatin, N.T., Hong Kong

ARTICLE INFO

Article history:
Received 20 April 2018
Revised 5 July 2018
Accepted 25 September 2018
Available online 4 October 2018

Communicated by Rongni Yang

Keywords:
Communication latency
Deep learning
Synchrophasor
Transient stability assessment.

ABSTRACT

Transient stability assessment is critical for power system operation and control. Existing related research makes a strong assumption that the data transmission time for system variable measurements to arrive at the control center is negligible, which is unrealistic. In this paper, we focus on investigating the impact of data transmission latency on synchrophasor-based transient stability assessment. In particular, we employ a recently proposed methodology named synchrophasor recovery and prediction framework to handle the latency issue and make up missing synchrophasors. Advanced deep learning techniques are adopted to utilize the processed data for assessment. Compared with existing work, our proposed mechanism can make accurate assessments with a significantly faster response speed.

1. Introduction

Transient stability assessment (TSA) is critical for the operation and control of power systems. With the ever-increasing demand in modern power grids, the transient stability issue is considered more serious than before because grids are operating close to their stability limits [1]. Power blackouts and significant system failures are two possible outcomes of this issue. Much research has been carried out on how to assess the stability status of a power system subject to large disturbances. With the assessment result, system operators can plan remedial control actions to maintain grid stability.

All existing TSA mechanisms require full or partial knowledge of the system operating state to conduct assessments [2]. With the assistance of wide-area monitoring systems (WAMS), this requirement can be fulfilled in real-world power systems [3,4]. Conventional mechanisms introduce an "observation window" in the assessment process, in which system variable dynamics are collected by measurement devices in the power system – see [5,6] for examples. Transient stability status is assessed after the window, and the assessment accuracy is highly dependent on the window length. The longer the observation window is, the more information is collected, which can result in better performance. However, this scheme has three major drawbacks. First, no preliminary results can be developed during the observation window. This significantly increases the system response time. Second, there appears to be no general rule of thumb to set the length of observation window. Since there is a trade-off between the assessment accuracy and response speed for TSA, it is hard to determine the optimal window length. Third, this scheme makes an implicit assumption when evaluating the response time of TSA mechanisms: all system measurements are immediately received by the control center through communication infrastructures without any latency.

In the past few years, results have been published on developing a "continuous observation" scheme to substitute the observation window – see [2,7] for examples. In this scheme, preliminary assessments are made once the first post-contingency system state is received at the control center, and subsequent assessments are conducted upon subsequent system measurements. In such a way, the first two drawbacks of the "observation window" scheme can be resolved. However, this scheme cannot relax the assumption that there is no communication latency [8]. When applied to real-world environments, this latency significantly increases the system response time. TSA mechanisms have to wait for the arrival of the last measurement, whose data packet may experience latency spikes or packet drop issues during transmission [9,10]. Therefore, it is necessary to develop a delay-aware TSA mechanism to handle the asynchronous arrival pattern of measurements and provide fast assessments.

Recently, a synchrophasor recovery and prediction framework (SRPF) was proposed to handle the communication latency of sys-

* Corresponding author.
E-mail addresses: jqyu@eee.hku.hk (J.J.Q. Yu), dhill@eee.hku.hk (D.J. Hill), albert@fano.ai (A.Y.S. Lam).

https://doi.org/10.1016/j.neucom.2018.09.059
0925-2312/

tem measurements in power system applications [8]. SRPF employs recent deep learning techniques to recover missing synchrophasors in the past, and make predictions of system states in the future. This is achieved by constructing a deep neural network (DNN) ensemble to learn the power system characteristics using historical and simulated time-domain system dynamics [8]. The temporal and spatial data correlation can be extracted from the processed data with DNN [11,12], and employed to recover missing data in real-time.

While SRPF is capable of providing system states in the near future, as will be discussed in Section 3.5, the system cannot be employed to handle TSA. In this work, we propose a new transient stability assessment mechanism based on SRPF and DNN to provide reliable and fast TSA results. In the proposed mechanism, upon receiving any post-contingency measurements at the control center, SRPF is employed to fill in the other measurements which have not yet been received due to communication latency, and also predict possible future system states. After the measurement recovery and prediction process, the synthetic data is employed to predict the post-contingency stability status of the power system using a DNN-based TSA system. Furthermore, we conduct comprehensive simulations to evaluate the efficacy of the proposed mechanism.

The rest of this paper is organized as follows. Section 2 analyzes the latency issue in transient stability assessment process. Section 3 elaborates on the formulation and implementation of the proposed delay aware TSA mechanism. Section 4 demonstrates case studies and numerical results on two test system. Finally this paper is concluded in Section 5 with a discussion of potential future research.

2. Delay aware transient stability assessment

In this work, we follow [8] to analyze the communication latency in WAMS. We consider the scenario in which synchronized phasor measurement units (PMU) sample system variables at a constant frequency, e.g., 60 Hz. Samples at time t from PMU $p \in \mathcal{P}$ are sent to the control center through communication infrastructures, which impose a stochastic latency $d_{p,t}$. Previous synchrophasor-based work assumed that $d_{p,t} \equiv 0$. Therefore, the system response time is developed by $n\Delta t + t'$, where n is the length of observation window, Δt is the length of each cycle, and t' is the computation time for TSA.

However, the latency values are actually stochastic, rendering samples from different PMUs measured at the same time to arrive in an asynchronous and disordered pattern. As a result, the system state at t remains incomplete until $\max_{p\in\mathcal{P}} d_{p,t}$. This delay must be included when calculating system response time. In addition, it is possible that some data packets experience packet drops or latency spikes in the communication network, rendering uncommonly high latency [9,10,13]. In such cases, the system response time of conventional mechanisms becomes unpredictable. Previous work [2,7] focuses on reducing the $n\Delta t$ component in the response time. However, the proposed mechanisms still assume a zero delay environment.

In this work, the proposed mechanism performs TSA in an iterative manner after fault clearance. Since measurements arrive at the control center in an asynchronous manner, SRPF is adopted to recover the missing measurements and predict potential future system states. Utilizing this information, recent advances in deep learning techniques are employed to develop the assessment results. The proposed mechanism copes with the asynchronous arrival of power system measurements, and is robust against latency spikes in communication networks.

3. SRPF-based transient stability assessment

In this section, we first briefly introduce the system model and SRPF methodology. Then we present the proposed SRPF and DNN-based delay aware TSA mechanism.

3.1. System model

In modern power systems, WAMS samples the power system states continuously in terms of system variable measurements. The system state at time instance t is represented by S_t, which consists of voltage magnitudes and angles of all buses in the network. In addition, M_t is adopted to denote the collection of all system variable measurements sampled by sampling units, e.g., phasor measurement units (PMU). The system topology and parameters of the power grid can be reflected by $h(\cdot)$, and $S_t = h(M_t)$.

At time t, $\{M_t, M_{t-1}, M_{t-2}, \ldots\}$ may be incomplete due to communication latency. M_t^- is introduced to represent the (incomplete) received measurements in M_t, and $S_t^- = h(M_t^-)$ is the incomplete system state that is subsequently calculated with M_t^-. The objective of the proposed TSA mechanism is to assess the post-contingency system stability using $\{S_t^-, S_{t-1}^-, S_{t-2}^-, \ldots\}$. Instead of directly investigating the characteristics of these incomplete measurements and system states, SRPF is firstly adopted to recover the missing measurements and predict the possible future system states. In such a way, the volume of available information for TSA is expanded.

3.2. Synchrophasor recovery and prediction framework

SRPF [8] is a recently proposed framework which aims to recover the missing measurements caused by communication latencies, and predict potential future system states based on available measurements. Specifically, SRPF employs $\{M_t^-, M_{t-1}^-, M_{t-2}^-, \ldots\}$ to recover $\{S_t, S_{t-1}, S_{t-2}, \ldots\}$ and predict $\{S_{t+1}, S_{t+2}, \ldots\}$ at time t. This objective is achieved by the two sub-systems defined in SRPF, namely, *Predictor* and *Estimator*. The predictor is designed to utilize multiple consecutive complete system states to predict the next system state. And the estimator is designed to combine this predicted system state with existing incomplete measurements of the same time instance. SRPF employs these two systems in an iterative manner to progressively generate recovered and predicted system states for other power system applications.

3.2.1. Predictor implementation

The predictor takes a sequence of complete system states as inputs, and predicts the possible system state at the next time instance:

$$S_{t+1}^+ = \text{Predictor}(S_t, S_{t-1}, S_{t-2}, \ldots), \tag{1}$$

where S_{t+1}^+ is the predicted system state at time $t+1$. In [8], predictor is implemented using DNN, namely a Gated Recurrent Unit (GRU) ensemble [14]. In the ensemble, multiple deep GRU networks are constructed, each of which can individually provide a predicted system state with the input ones. The results are averaged in order to improve the robustness of the system against data noises [15].

GRU [16] is a modern model of artificial neural networks (ANN) [17,18], which simulates the model of a given system by learning from the input-output relationship of the system. While conventional ANN only extracts the spatial data correlation from the input training data, GRU additionally learns the system characteristics from the temporal data correlation [16]. This is achieved by introducing a series of training parameters which maps the time-series input data $x_1, x_2, \ldots, x_t$ into a sequence of output data $h_1, h_2, \ldots, h_t$ using the following equations:

$$z_t = \text{sigm}(W_{xz}x_t + W_{hz}h_{t-1} + b_z), \tag{2a}$$

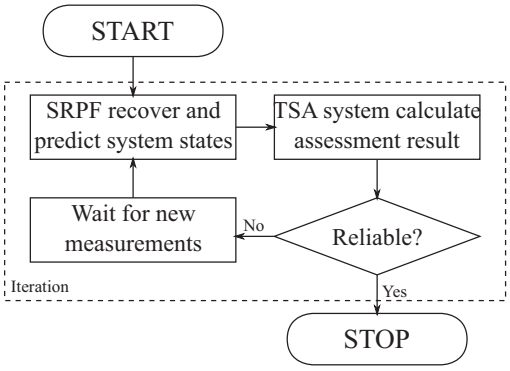

Fig. 1. Flow chart of the proposed TSA mechanism.

$$r_t = \text{sigm}(W_{xr}x_t + W_{hr}h_{t-1} + b_r), \tag{2b}$$

$$h_t = z_t \odot h_{t-1} + (1 - z_t) \odot \tanh(W_{xh}x_t + W_{hh}(r_t \odot h_{t-1}) + b_h), \tag{2c}$$

where z_t and r_t are intermediate values, W_{xz}, W_{hz}, W_{xr}, W_{hr}, W_{xh}, and W_{hh} are weight parameters, b_z, b_r, and b_h are bias parameters, sigm$(\cdot)$ is the sigmoid function, and $\odot$ is the element-wise multiplication operation. Eq. (2) calculates output h_t at the tth time instance using input data x_t, training parameters (weight and bias), and the output h_{t-1} of the previous time instance. Consequently, given a sequence of time-series data, GRU can iteratively employ (2) to calculate the outputs with input data and training parameters. In SRPF, the inputs are the history system states $\{S_t, S_{t-1}, S_{t-2}, \ldots\}$, and outputs are the state at the next time instance, i.e, S_{t+1}. The training process can be conducted using real historical or time-series simulation data, and the trained parameters are used to make predictions in real-time with (2).

3.2.2. Estimator implementation

One may note that the predictor takes the complete system states as inputs and outputs the predicted system state at the next time instance. This means that some of the actual measurements in this and future time instances may be partially available at the control center. The estimator combines the predicted state with the already available measurements to give an estimation of the real system state at the same time instance:

$$\hat{S}_{t+1} = \text{Estimator}(S^+_{t+1}, S^-_{t+1}, S^-_{t+2}, \ldots), \tag{3}$$

where $\hat{S}_{t+1}$ is the estimated system state for $t+1$, and is expected to be more accurate than S^+_{t+1} in approximating S_{t+1}. In [8], a simplistic estimator implementation is proposed, which fills the missing state variables in S^-_{t+1} with the corresponding values in S^+_{t+1} to develop $\hat{S}_{t+1}$. This implementation, as demonstrated in [8], is simple yet can develop satisfactory results in terms of estimation accuracy when estimating the power system states.

3.3. Proposed mechanism

In this paper, we incorporate the "time-adaptive" idea presented in [2,7] and propose a delay aware TSA mechanism which aims to provide accurate TSA results at the earliest possible time. The proposed mechanism performs TSA in an iterative manner, in which preliminary assessment results are developed in each iteration. The flow chart of the mechanism is depicted in Fig. 1.

Upon detecting a contingency, the mechanism starts assessing post-contingency system transient stability. In each iteration,

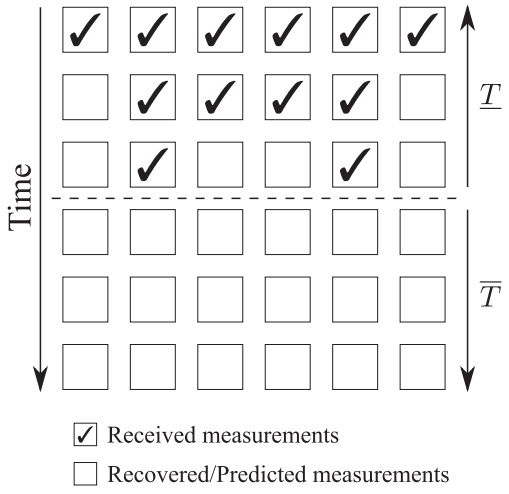

Fig. 2. Output data of SRPF and input data of DNN for TSA.

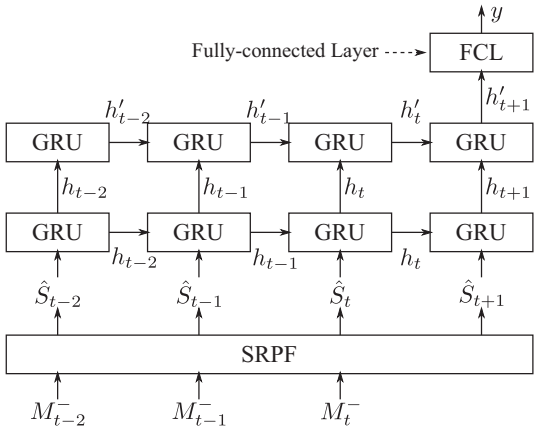

Fig. 3. SRPF and DNN layers. In this figure, parameters $\underline{T} = 3$ and $\overline{T} = 1$.

SRPF is firstly adopted to pre-process synchrophasor measurements available at the control center. In this process, the history system states of the past $\underline{T}$ cycles are estimated, and those of future $\overline{T}$ cycles are predicted, where $\underline{T}$ and $\overline{T}$ are control parameters whose sensitivity will be investigated in Section 4.2. Fig. 2 presents the output system states of SRPF, which also corresponds to the input data of the subsequent DNN. Using these system states, a new TSA system calculates the preliminary assessment result and its reliability. If the result is reliable, the mechanism outputs it for further remedial and protective control actions. Otherwise, the mechanism waits for new system measurements to arrive at the control center. This process iterates until a reliable TSA result is developed.

From Fig. 1 it is obvious that the accuracy of the TSA system is critical to the performance of the mechanism. In this work, DNN is employed to construct the system. Two GRU layers (each with 512 units) and a fully connected neuron layer (with 128 nodes) are stacked to form the DNN for TSA as shown in Fig. 3. Upon receipt of the recovered and predicted system states from SRPF, the data is input into (2) to calculate the first intermediate states $\{h_{t-\underline{T}+1} \cdots, h_{t-1}, h_t, h_{t+1}, \ldots, h_{t+\overline{T}}\}$. After the calculation, (2) with a different set of training parameters are employed to further process the intermediate states, and develop $\{h'_{t-\underline{T}+1} \cdots, h'_{t-1}, h'_t, h'_{t+1}, \ldots, h'_{t+\overline{T}}\}$. Finally, the last value $h'_{t+\overline{T}}$ is input into a fully-connected neuron layer [19] with a sigmoid activation function to translate the intermediate state into a human-readable transient stability index y between zero and one. An index smaller than a control parameter Θ represents that the

mechanism considers the system to be transiently stable subject to the contingency, and greater than $1-\Theta$ means that the system will become unstable in the future. If the index is between Θ and $1-\Theta$, the mechanism cannot make a credible assessment at the current time, and new measurements are required to make further assessments.

Comparing with conventional TSA methods such as time-domain simulation [20] and transient energy function [21,22], neural network-based TSA systems have two major advantages [2]:

- Network training process is typically conducted offline, which means that the online testing calculation is computationally efficient, i.e., less time is required to develop TSA results [23].
- Neural networks try to emulate the system response with only input power dynamic data (historical and/or simulated) [24]. Therefore, accurate power system models and parameters are not required.

3.4. Network training

In Section 3.3, the proposed mechanism is employed to develop real-time TSA results given incomplete power system measurements. However, the calculation process includes (2), in which multiple training parameters need to be optimized before implementation. In this section, the data and method adopted to train these parameters are discussed.

In the proposed mechanism, training data are employed to fine tune the training parameters in GRU and full-connected layers. The data can be generated with time-domain simulation on post-contingency power system dynamics, and historical dynamics recorded during operation can also be employed. Specifically, using 50/60 Hz sampling, post-contingency positive sequence voltage magnitudes and angles of all buses can be arranged in the following form as inputs:

$$\begin{bmatrix} V_{1,\underline{T}} & V_{2,\underline{T}} & V_{3,\underline{T}} & \cdots & V_{N,\underline{T}} \\ V_{1,\underline{T}-1} & V_{2,\underline{T}-1} & V_{3,\underline{T}-1} & \cdots & V_{N,\underline{T}-1} \\ \vdots & \vdots & \vdots & & \vdots \\ V_{1,\overline{T}} & V_{2,\overline{T}} & V_{3,\overline{T}} & \cdots & V_{N,\overline{T}} \end{bmatrix} = \begin{bmatrix} \hat{S}_{\underline{T}} \\ \hat{S}_{\underline{T}-1} \\ \vdots \\ \hat{S}_{\overline{T}} \end{bmatrix}$$

where N is the number of buses in the system, and $V_{i,t}$ is the estimated voltage phasor of bus i at time instance t from SRPF (See Fig. 3 for reference).

To tune the training parameters, the expected output of the neural network must also be provided along with the input data. In the proposed TSA mechanism, the output, i.e., y in Fig. 3, is obtained by calculating the post-contingency maximum angle deviation $\delta_{\max}$ of any two generators:

$$y = \begin{cases} 1 \text{ (Unstable)} & \text{for } \delta_{\max} \geq 360 \\ 0 \text{ (Stable)} & \text{otherwise} \end{cases}. \tag{4}$$

This assignment is widely adopted in the previous literature, see [2,7,25] for examples.

Given a collection of C training cases $\{\hat{S}^{(c)}_{\underline{T}}, \hat{S}^{(c)}_{\underline{T}-1}, \ldots, \hat{S}^{(c)}_{\overline{T}}, y^{(c)}\}_{i=1}^{C}$, the objective of the training process is to find the optimal training parameter values such that the binary cross entropy error function is minimized:

$$\text{minimize} - \sum_{n=1}^{C} [y^{(c)} \log \hat{y}^{(c)} + (1 - y^{(c)}) \log(1 - \hat{y}^{(c)})], \tag{5}$$

where $\hat{y}^{(c)}$ is the assessment result using the input data $\{\hat{S}^{(c)}_{\underline{T}}, \hat{S}^{(c)}_{\underline{T}-1}, \ldots, \hat{S}^{(c)}_{\overline{T}}\}$ and the training parameters. This optimization problem can be effectively solved using existing gradient-based solutions, and in this work the Adam optimizer [26] is adopted due to its fast convergence speed.

3.5. Discussion

In this work, we employ SRPF in [8] to develop system states in near future, which can be utilized in a DNN to further estimate the transient stability of the power grid. In fact, it is hypothetically possible to use SRPF to predict more future states and then calculate the stability using (4). However, the prediction error of SRPF may limit this usage of the system. By observing the case studies in [8], it is clear that the accuracy of the predicted system states, while remaining satisfactory, decreases with the predicted time in the future. TSA typically can lead to a large enough angle deviation to make the system out-of-sync, but the deviation is not significant enough in the first several cycles after fault clearances. On the other hand, SRPF aims to provide the future system states in a power grid, which cannot be directly used to calculate the generator angle deviations. Therefore, SRPF alone is not capable of identifying TSA at the early stage, making this research necessary.

Furthermore, we mainly focus on developing a well-performing TSA technique based on SRPF in this paper. The assessment accuracy and computation time performance are evaluated through comprehensive case studies, which will be presented in Section 4. In the meantime, it is possible to develop related theoretical analyses on performance bounds of the proposed technique in two aspects, namely, the performance guarantees of SRPF on synchrophasor recovery accuracy and transient assessment accuracy. These studies are out of the scope of this paper and will be thoroughly investigated in the future work.

4. Case study

To evaluate the performance of the proposed delay aware TSA mechanism, a comprehensive case study is conducted to analyze its characteristics. Specifically, we first compare the TSA accuracy and response speed with existing state-of-the-art algorithms in the literature. Then the parameter sensitivities of three control parameters ($\underline{T}$, $\overline{T}$, Θ) in the mechanism are studied. After that, we examine the robustness of the proposed mechanism when experiencing different latency patterns and data noises. In addition, a large scale power system is also employed to test the scalability of the mechanism.

The New England 10-machine system benchmark [27] is employed in the simulations, which comprises 39 buses, 10 synchronous generators, 34 transmission lines, and 12 transformers. Among all generators, G10 represents the aggregated generation from the external grid. All other generators are equipped with an IEEE Type-1 (IEEET1) exciter [28] and a WSCC Type G (BPA_GG) governor with parameters taken from [29]. This setting accords with previous work by the authors [2,25].

In the simulation, the training and testing data are generated by time-domain simulation of post-contingency power system dynamics, which includes all possible $N-1$ contingencies and selected $N-2$ contingencies subject to a three-phase short-circuit fault with a random fault clearance time between 0.1 and 0.3 s [8]. In total, 5000 transient contingencies are generated in the test with a random load level between 80% and 120% of the nominal case, and the power system dynamics are simulated using DIgSILENT PowerFactory [30]. All simulations are conducted on a computer with an Intel Core i7 CPU at 3.60 GHz clock speed. The deep neural networks are trained with an nVidia GTX 1080 graphics card.

Furthermore, we employ the real latency values from FNET/Grid Eye records [31] in this work. All synthetic measurements with the same timestamp are randomly selected from the same time record in [31]. For cross-validation, in this work all generated system dynamics are randomly divided into a training dataset and a testing dataset with a 3:1 ratio. As a result, 3750 random cases are used

Table 1
Comparison of assessment accuracy and response time.

Technique	Testing dataset				Training dataset			
	Accuracy	Avg. time	Min. time	Max. time	Accuracy	Avg. time	Min. time	Max. time
Proposed	**100.0%**	**40.6 ms**	**22.1 ms**	89.7 ms	**99.8%**	**39.4 ms**	**21.9 ms**	**121.5 ms**
[25]	**100.0%**	50.8 ms	39.0 ms	**82.6 ms**	**99.8%**	49.1 ms	28.8 ms	150.3 ms
[2]	99.9%	92.5 ms	57.2 ms	138.1 ms	**99.8%**	91.2 ms	44.4 ms	151.0 ms
[7]	99.4%	87.1 ms	59.9 ms	147.5 ms	–	–	–	–

for training the neural network in the proposed mechanism, and the remaining 1250 cases are employed to test the system performance. The same configuration is adopted in previous work, see [2,7,8] for examples. This setting can effectively reveal over-fitting issues, which result in performance difference on the training and testing datasets.

4.1. TSA accuracy and response time

In the first test, the TSA result accuracy and averaged response time are evaluated and compared with representative existing TSA algorithms in the literature. In the simulation, control parameters are set to the following values: $\underline{T} = 5,\ \overline{T} = 5,\ \Theta = 0.4$. Specifically, we adopt the algorithms proposed in [2,7,25] for comparison, which are among the fastest TSA mechanisms in the literature. We assume that the TSA techniques in [2,7] are conducted once the complete system states can be developed at the control center, since they do not consider the latency issue. For the compared algorithm proposed in [7], we further assume that the computation time is zero[1].

The simulation results are presented in Table 1. From the table it can be concluded that the proposed delay aware TSA mechanism outperforms existing fast TSA techniques in both assessment accuracy and response speed. Specifically, the proposed mechanism yields satisfactory TSA accuracy in both training and test datasets, which illustrates that it does not suffer from the over-fitting problem. In addition, it can also develop assessment results earlier than the previous technique which also considers communication delays, i.e., [25]. This is contributed by both the accurate recovered and predicted system states generated by SRPF and the outstanding learning capability of the employed DNN [8]. One may note that the proposed mechanism improves the average response time of TSA by approximately 10 milliseconds compared with the existing fastest solution, which is relatively insignificant. We will demonstrate in the subsequent sections that the proposed mechanism is more robust when handling different measurement data.

Besides the average simulation results, it is also of interest to study the distribution of TSA response time for the compared techniques. In Fig. 4, the response time statistics for the proposed mechanisms introduced in [2,25] on the 1250 testing cases are presented with a granularity of 10 milliseconds. The x-axis is the elapsed real time after fault clearance, and the y-axis represents the ratio of all test cases for which the respective technique can develop a TSA result within the corresponding given time. From the figure it can be observed that the proposed mechanism is faster than the compared ones in term of system response speed. This can be interpreted as that given a random unknown post-contingency power system dynamics, the proposed mechanism generally requires less time to develop a TSA result than others. This observation also accords with the results presented in Table 1.

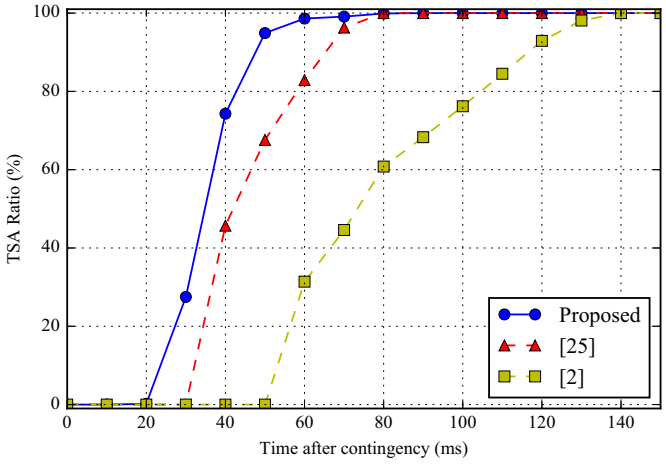

Fig. 4. TSA response time and ratio comparison.

4.2. Parameter sensitivity analysis

In all previous tests, a fixed combination of the control parameters are adopted, i.e., $\underline{T} = 5,\ \overline{T} = 5,$ and $\Theta = 0.4$. However, it remains unknown if this combination yields the best system performance, and how the mechanism would respond to parameter changes. In this section, a parameter sweep test is performed to find the best performing control parameters. To be specific, the TSA accuracy and response time are compared for $\{\underline{T}, \overline{T}\} \in \{\{3,3\},\{5,5\},\{7,7\},\{9,9\}\}$ and $\Theta \in \{0.25,\ 0.30,\ 0.35,\ 0.40,\ 0.45\}$ on the testing dataset[2]. The simulation results are presented in Table 2.

From the table it can be observed that the previously adopted parameters ($\underline{T} = 5,\ \overline{T} = 5,\ \Theta = 0.4$) can yield the best performance considering the trade-off between accurate TSA results and fast TSA speed. In general, small Θ values (less than 0.35) develop inferior accuracy and response speed. This is because a small Θ value will drive the proposed mechanism iterate more to generate a "reliable" result, rendering longer system response time. In addition, these results also indicate that the extra iterations actually undermines TSA accuracy. This implies that these iterations introduce less relevant system dynamics information into the system.

Another observation is on the relationship between $\{\underline{T}, \overline{T}\}$ and the system performance. Generally speaking, medium $\{\underline{T}, \overline{T}\}$ values lead to more accurate TSA results, and the response time increases with the values. On the one hand, a small $\{\underline{T}, \overline{T}\}$ pair requires less computation time for SRPF to make recoveries and predictions. But insufficient system dynamics information is supplied to the TSA system, and a worse TSA accuracy value can be observed. On the other hand, a large $\{\underline{T}, \overline{T}\}$ pair provides more system information for assessment. However, more time is consumed by SRPF, and

[1] The system response time values presented in case studies include both the communication latency and the computation time of the respective mechanism.

[2] Due to page limit, $\underline{T}$ and $\overline{T}$ are grouped as one pair of parameters. Investigations show that the system performance are quite similar if their values are changed so that $\underline{T} + \overline{T}$ remains constant.

Table 2
TSA accuracy and response time for different control parameters.

	$\{\underline{T}, \overline{T}\}$	TSA accuracy				Average response time			
		{3, 3}	{5, 5}	{7, 7}	{9, 9}	{3, 3}	{5, 5}	{7, 7}	{9, 9}
Θ	0.25	90.3%	95.0%	92.3%	84.5%	59.8 ms	68.9 ms	71.0 ms	76.7 ms
	0.30	97.2%	99.9%	99.2%	99.4%	60.4 ms	64.1 ms	71.9 ms	72.9 ms
	0.35	98.5%	**100.0%**	99.8%	99.5%	45.4 ms	46.0 ms	51.7 ms	61.3 ms
	0.40	98.3%	**100.0%**	**100.0%**	99.3%	38.8 ms	40.6 ms	44.1 ms	48.9 ms
	0.45	89.6%	98.7%	97.1%	93.2%	30.0 ms	32.9 ms	35.4 ms	37.0 ms

Table 3
Impact of different latencies.

Technique	Latency	Accuracy(%)	Avg. time (ms)	Min. time (ms)	Max. time (ms)	Slowdown
Proposed	High latency	100.0	55.21	30.05	121.98	1.360
	Lossy link	100.0	42.88	23.34	94.73	1.056
	Bad link	100.0	57.76	31.44	127.62	1.423
[25]	Highlatency	100.0	71.25	54.70	115.85	1.402
	Lossy link	99.5	69.48	53.34	112.98	1.368
	Bad link	99.4	84.63	64.97	137.61	1.666
[2]	High latency	99.9	137.38	84.95	205.10	1.485
	Lossy link	99.4	178.78	110.55	266.92	1.933
	Bad link	99.3	185.61	114.78	277.11	2.007
[7]	High latency	99.4	130.50	89.75	221.00	1.498
	Lossy link	99.4	166.82	114.72	282.50	1.915
	Badlink	99.3	176.68	121.51	299.20	2.028

the extra information may actually introduce more data noise in the system, rendering a worse assessment accuracy performance. Therefore, {5, 5} is suggested by the parameter sweep as the optimal values for $\{\underline{T}, \overline{T}\}$ considering the system performance.

4.3. Impact of different latency patterns

In real-world applications, various WAMS can have different underlying communication infrastructures, rendering different latency values. In this test, the impact of this factor on the assessment speed and accuracy is investigated. Specifically, we modify the benchmark latency data employed in Section 4.1 (tagged as "benchmark") and develop the following scenarios for analyses:

- *Highlatency*: All latencies are increased by 50% from their benchmark value. This scenario emulates WAMS with high latency but stable communication links.
- *Lossy link*: All latencies retain their benchmark value, but random 30% of the measurements have their latency values increased by 100%. This scenario emulates WAMS with unstable communication links.
- *Bad link*: All latencies are increased by 50% from their benchmark values, and 30% of the measurements have their latency values increased by 100%. This scenario combines the previous two to emulate a quite bad communication infrastructure. It can be considered as a worst case scenario.

Other experimental configurations are identical as in Section 4.1 and the simulation results are presented in Table 3. In this table, the TSA results on the 1250 test cases are presented. The average, minimum, and maximum system response times are listed, together with the averaged slowdown of the respective latency compared with the benchmark scenario in Section 4.1. A smaller slowdown value indicates that the respective mechanism is less influenced by the changed latency.

From the table it can be concluded that while the system response speed is negatively influenced by the increase of communication latency, the proposed mechanism can still develop TSA results within a satisfactory period of time. Specifically, the system response time is notably influenced in the *High Latency* and *Bad Link* scenarios, in which the communication latencies are stable and slow. In the meantime, although the average measurement latency is increased by 30% in the *Lossy Link* scenario, the response time slowdown compared with the benchmark scenario is not significant. This demonstrates the capability of the proposed mechanism in handling unstable communications of WAMS, contributed by the data pre-processing of SRPF. In addition, it can be observed that the assessment accuracy remains 100% for different latency values, which presents the outstanding transient stability identification capability.

Furthermore, we also adopt the previous TSA techniques and test them with the different scenarios. The simulation results are compared in Table 3. It can be observed that both techniques can handle the *High Latency* scenario with a reasonable response time slowdown. However, the performance deteriorates if random measurements experience latency spikes. This is due to the design of the respective techniques. In [25], TSA is conducted based on a "main block", which can accept system states with data loss, and multiple "ensemble blocks", which require the complete data of a pre-defined subset of system states. Hence when latency spikes delay the measurements, these "ensemble blocks" need to wait for their arrival before making assessments, rendering a slow response time. For the techniques in [2,7], complete system states are always required by the systems. Therefore they also suffer from the same problem. From this comparison it can be concluded that the proposed TSA outperforms the compared techniques, especially when the communication latency in WAMS is unstable.

4.4. Measurement noise sensitivity test

In the previous analyses, it is assumed that the measurements developed by WAMS can accurately reflect the system state, i.e., no data noise is recorded. In the meantime, these synchrophasors suffer from sampling error issues in practice [2]. According to IEEE Standard for Synchrophasor Data Transfer for Power Systems (C37.118.2–2011) [32], the total vector error (TVE) for all synchrophasors complying with the standard should be no greater than 1%, and many existing PMUs can achieve the accuracy, see [33] for an example. In this section, we investigate the impact of random sampling error on the performance of the proposed TSA mechanism. We follow the approach in [2,34] to construct noisy

Table 4
Accuracycomparison with noisy measurements.

Technique	ϵ			
	0.2%	0.5%	1.0%	2.0%
Proposed	100.0%	100.0%	100.0%	99.9%
[25]	100.0%	99.9%	99.9%	99.6%
[2]	99.9%	99.9%	99.8%	99.4%

Table 5
Results on 50-generator 145-bus system.

Dataset	Accuracy(%)	Avg. time (ms)	Min. time (ms)	Max. time (ms)
Testing	100.0	51.2	34.0	121.3
Training	99.9	50.9	36.4	130.4

power system dynamics data based on the benchmark training and testing cases. Specifically, a noise phasor $\Delta V\angle\Delta\theta$ is randomly sampled from a truncated complex Gaussian distribution for each measurement:

$$\mathbb{P}(\Delta V\angle\Delta\theta|0,\epsilon^2) = \begin{cases} 9\times(\pi(1-e^{-9})\epsilon^2|V\angle\theta|^2)^{-1}\exp(-\frac{9|\Delta V\angle\Delta\theta|^2}{\epsilon^2|V\angle\theta|^2}) \\ \qquad\qquad \text{if } |\Delta V\angle\Delta\theta| \le \epsilon|V\angle\theta| \\ 0 \qquad\qquad \text{otherwise} \end{cases}, \tag{6}$$

where $V\angle\theta$ is the simulated voltage phasor, and ϵ is the expected maximum total vector error. Then the new noisy voltage phasor $\tilde{V}\angle\tilde{\theta}$ can be calculated by imposing the noise phasor on the original one:

$$\tilde{V}\angle\tilde{\theta} = V\angle\theta + \Delta V\angle\Delta\theta. \tag{7}$$

The noisy data is employed for both training and testing the proposed mechanism, and all other simulation configurations remain the same from previous tests.

The simulation results on the testing cases are presented in Table 4. In this test, ϵ is set to 0.2%, 0.5%, 1.0%, and 2.0% to emulate PMUs with difference levels of accuracy. The simulation results of the techniques in [2,25] on the same data are also presented for reference. From the table, it can be observed that the assessment accuracy is slightly undermined by the data noise when the noise ratio is notable (2%), yet the performance degradation is miniscule. Furthermore, if PMUs are designed to comply with the IEEE C37.118.2–2011 standard, the proposed mechanism is not influenced by data noises. To conclude, the proposed SRPF-based TSA mechanism can achieve perfect assessment accuracy when PMUs provide reasonably accurate measurements, and can still achieve satisfactory assessment performance when analyzing data with significant noises.

4.5. Large power system test

In all the previous simulations, the New England 10-machine system is employed, which is a relatively small power system. To evaluate the system performance of the proposed mechanism on large-scale systems, a large power system with 50 generators and 145 buses [35] is tested in this simulation. The same method to generate training and testing datasets is employed to develop 20,000 contingencies. The simulation is performed with the same configuration as in Section 4.1, and the results are presented in Table 5.

Compared with the results presented in Table 1, the system performance of the proposed mechanism on the large power system remains satisfactory. In both systems, the TSA accuracy on testing dataset is 100%. Meanwhile, as more information is required by TSA on large systems, the system response time in Table 5 is generally longer than that for New England 10-machine system. Despite this, the required time is still short enough to facilitate subsequent remedial control actions. Both results outline the high applicability of the proposed mechanism on large systems.

Besides the accuracy and system response time, it is worth noting that the training time for the system is also acceptable considering the dynamic changes in power systems. When employing the proposed mechanism in the New England 10-machine system, the total training time is less than 40 min. The time increases to approximately one hour for the 50-machine large system. The fast training speed also makes the proposed mechanism robust considering significant changes to the power grid, since the system can be quickly updated/re-trained online with new system measurements for performance improvement. The detailed implementation for the re-training process is beyond the scope of this paper, and will be investigated in the future.

5. Conclusion

In this paper, a new TSA mechanism based on synchrophasor recovery and prediction framework (SRPF) and deep neural networks (DNN) is proposed to provide timely and accurate TSA results for power system control and operation. Compared with previous work, the proposed mechanism considers the stochastic communication latency, which is a critical factor in system response speed but usually overlooked in the literature. Specifically, upon receiving post-contingency power system variable measurements, the mechanism employs SRPF to recover other missing measurements which are still being transmitted. In addition, based on the recovered measurements, SRPF further develops future system states for assessment. The recovered and predicted system states are input into a deep GRU network-based TSA system for assessment. By extracting both spatial and temporal data correlations, the proposed system can develop accurate TSA results within a short computation time.

In order to evaluate the performance of the proposed TSA mechanism, the New England 10-machine system and a 50-generator 145-bus system are employed in the case studies. All simulations indicate that the proposed mechanism can achieve a satisfactory assessment accuracy with a short response time on different scales of power systems, considering communication latencies. In addition, the impact of different latency patterns on the proposed mechanism is investigated. The results reveal that the proposed mechanism can be applied to WAMS with bad communication infrastructures without significant performance degradation. Last but not least, the sensitivity of control parameters is studied through a parameter sweep test.

Future work will focus on two topics. The predictors employed in this work are the positive sequence voltage phasors. It is possible that a wide range of other predictors can develop better accuracy and/or response time [36]. In addition, in this work a GRU-based DNN is constructed as the TSA system. With the rapid development of deep learning techniques, new and advanced neural network structures can be adopted [37].

Acknowledgment

This work was supported by the Theme-based Research Scheme of the Research Grants Council of Hong Kong, under Grant No. T23-701/14-N.

References

[1] P. Kundur, J. Paserba, V. Ajjarapu, G. Andersson, A. Bose, C. Canizares, N. Hatziargyriou, D. Hill, A. Stankovic, C. Taylor, T.V. Cutsem, V. Vittal, Definition and classification of power system stability IEEE/CIGRE joint task force on stability terms and definitions, IEEE Trans. Power Syst. 19 (3) (2004) 1387–1401.

[2] J.J.Q. Yu, D.J. Hill, A.Y.S. Lam, J. Gu, V.O.K. Li, Intelligent time-adaptive transient stability assessment system, IEEE Trans. Power Syst. 33 (1) (2018) 1049–1058, doi:10.1109/TPWRS.2017.2707501.
[3] M. Begovic, D. Novosel, D. Karlsson, C. Henville, G. Michel, Wide-area protection and emergency control, Proc. IEEE 93 (5) (2005) 876–891.
[4] M. Zima, M. Larsson, P. Korba, C. Rehtanz, G. Andersson, Design aspects for wide-area monitoring and control systems, Proc. IEEE 93 (5) (2005) 980–996.
[5] T. Amraee, S. Ranjbar, Transient instability prediction using decision tree technique, IEEE Trans. Power Syst. 28 (3) (2013) 3028–3037.
[6] D. You, K. Wang, L. Ye, J. Wu, R. Huang, Transient stability assessment of power system using support vector machine with generator combinatorial trajectories inputs, Int. J. Elect. Power Energy Syst. 44 (1) (2013) 318–325.
[7] R. Zhang, Y. Xu, Z.Y. Dong, K.P. Wong, Post-disturbance transient stability assessment of power systems by a self-adaptive intelligent system, IET Gener. Trans. Distrib. 9 (3) (2015) 296–305.
[8] J.J.Q. Yu, A.Y.S. Lam, D.J. Hill, Y. Hou, V.O.K. Li, Delay aware power system synchrophasor recovery and prediction framework, IEEE Trans. Smart Grid (2018), doi:10.1109/TSG.2018.2834543. In press
[9] A. Hernandez, E. Magana, One-way delay measurement and characterization, in: Proceedings of the Third International Conference on Networking and Services, 2007. ICNS, 2007, pp. 114–119.
[10] Y. Wu, L. Nordström, D.E. Bakken, Effects of bursty event traffic on synchrophasor delays in IEEE C37.118, IEC61850, and IEC60870, in: Proceedings of the IEEE International Conference on Smart Grid Communications (SmartGridComm), 2015, pp. 478–484.
[11] Y. Yang, Y. Xu, J. Han, E. Wang, W. Chen, L. Yue, Efficient traffic congestion estimation using multiple spatio-temporal properties, Neurocomputing 267 (2017) 344–353, doi:10.1016/j.neucom.2017.06.017.
[12] J.J.Q. Yu, Y. Hou, A.Y.S. Lam, V.O.K. Li, Intelligent fault detection scheme for microgrids with wavelet-based deep neural networks, IEEE Trans. Smart Grid (2018), doi:10.1109/TSG.2017.2776310. In press
[13] J. Lai, H. Zhou, X. Lu, Z. Liu, Distributed power control for ders based on networked multiagent systems with communication delays, Neurocomputing 179 (2016) 135–143, doi:10.1016/j.neucom.2015.11.068.
[14] L.K. Hansen, P. Salamon, Neural network ensembles, IEEE Trans. Pattern Anal. Mach. Intell. 12 (10) (1990) 993–1001.
[15] C. Smith, Y. Jin, Evolutionary multi-objective generation of recurrent neural network ensembles for time series prediction, Neurocomputing 143 (2014) 302–311, doi:10.1016/j.neucom.2014.05.062.
[16] K. Cho, B. Van Merriënboer, C. Gulcehre, D. Bahdanau, F. Bougares, H. Schwenk, Y. Bengio, Learning Phrase Representations using RNN Encoder–decoder for Statistical Machine Translation, in: Proceedings of the Conference on Empirical Methods in Natural Language Processing (EMNLP),Doha, Qatar, 2014, pp. 1724–1734.
[17] R. Lippmann, An introduction to computing with neural nets, IEEE ASSP Mag. 4 (2) (1987) 4–22.
[18] J.J.Q. Yu, Y. Hou, V.O.K. Li, Online false data injection attack detection with wavelet transform and deep neural networks, IEEE Trans. Ind. Informat. 14 (7) (2018) 3271–3280, doi:10.1109/TSG.2017.2776310.
[19] R. Reed, R.J.M. II, Neural Smithing: Supervised Learning in Feedforward Artificial Neural Networks, A Bradford Book, 1999.
[20] P. Kundur, Power System Stability and Control, McGraw-Hill Education, 1994.
[21] I.A. Hiskens, D.J. Hill, Energy functions, transient stability and voltage behaviour in power systems with nonlinear loads, IEEE Trans. Power Syst. 4 (4) (1989) 1525–1533.
[22] A.-A.A. Fouad, V. Vittal, Power System Transient Stability Analysis using the Transient Energy Function Method, Prentice Hall, 1992.
[23] G. Li, L. Deng, L. Tian, H. Cui, W. Han, J. Pei, L. Shi, Training deep neural networks with discrete state transition, Neurocomputing 272 (2018) 154–162, doi:10.1016/j.neucom.2017.06.058.
[24] K.S. Narendra, K. Parthasarathy, Identification and control of dynamical systems using neural networks, IEEE Trans. Neural Netw. 1 (1) (1990) 4–27.
[25] J.J.Q. Yu, A.Y.S. Lam, D.J. Hill, V.O.K. Li, Delay aware intelligent transient stability assessment system, IEEE Access 5 (2017) 17230–17239, doi:10.1109/ACCESS.2017.2746093.
[26] D. Kingma, J. Ba, Adam: a method for stochastic optimization, in: Proceeding of the Third International Conference for Learning Representations, San Diego, 2015.
[27] A. Pai, Energy Function Analysis for Power System Stability, Springer Science & Business Media, 1989.
[28] IEEE Recommended Practice for Excitation System Models for Power System Stability Studies, IEEE Std 421.5–2005, 2006.
[29] P. Demetriou, M. Asprou, J. Quiros-Tortos, E. Kyriakides, Dynamic IEEE test systems for transient analysis, IEEE Syst. J. 11 (4) (2017) 2108–2117".
[30] PowerFactory - DIgSILENT Germany, 2018 (http://www.digsilent.de/index.php/products-powerfactory.html).
[31] FNET server web display, 2018, FNET.
[32] , IEEE Standard for Synchrophasor Data Transfer for Power Systems, IEEE Std C37.118.2–2011, IEEE Std, 2011.
[33] GE Grid Solutions, 2018 (http://www.gegridsolutions.com/).
[34] M. He, V. Vittal, J. Zhang, Online dynamic security assessment with missing pmu measurements: A data mining approach, IEEE Trans. Power Syst. 28 (2) (2013) 1969–1977.
[35] V. Vittal, Transient stability test systems for direct stability methods, IEEE Trans. Power Syst. 7 (1) (1992) 37–43.
[36] I. Kamwa, S. Samantaray, G. Joos, Development of rule-based classifiers for rapid stability assessment of wide-area post-disturbance records, IEEE Trans. Power Syst. 24 (1) (2009) 258–270.
[37] Y. LeCun, Y. Bengio, G. Hinton, Deep learning, Nature 521 (7553) (2015) 436–444.

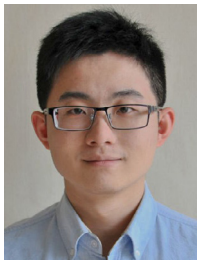

James J.Q. Yu received the B.Eng. and Ph.D. degree in Electrical and Electronic Engineering from the University of Hong Kong, Pokfulam, Hong Kong, in 2011 and 2015, respectively. He is currently an honorary assistant professor and post-doctoral fellow at the Department of Electrical and Electronic Engineering, The University of Hong Kong. He is also the Chief Research Consultant of GWGrid Inc. and Fano Labs. His research interests include smart city technologies, deep learning and big data industrial applications, and evolutionary computation.

David J. Hill received the Ph.D. degree in Electrical Engineering from the University of Newcastle, Australia, in 1976. He holds the Chair of Electrical Engineering in the Department of Electrical and Electronic Engineering at the University of Hong Kong. He is also a part-time Professor of Electrical Engineering at The University of Sydney, Australia. During 2005–2010, he was an Australian Research Council Federation Fellow at the Australian National University. Since 1994, he has held various positions at the University of Sydney, Australia, including the Chair of Electrical Engineering until 2002 and again during 2010–2013 along with an ARC Professorial Fellowship. He has also held academic and substantial visiting positions at the universities of Melbourne, California (Berkeley), Newcastle (Australia), Lund (Sweden), Munich and in Hong Kong (City and Polytechnic). His general research interests are in control systems, complex networks, power systems and stability analysis. His work is now mainly on control and planning of future energy networks and basic stability and control questions for dynamic networks. Professor Hill is a Fellow of the Society for Industrial and Applied Mathematics, USA, the Australian Academy of Science, the Australian Academy of Technological Sciences and Engineering and the Hong Kong Academy of Engineering Sciences. He is also a Foreign Member of the Royal Swedish Academy of Engineering Sciences.

Albert Y.S. Lam received the B.Eng. degree (First Class Honors) in Information Engineering and the Ph.D. degree in Electrical and Electronic Engineering from the University of Hong Kong (HKU), Hong Kong, in 2005 and 2010, respectively. He was a postdoctoral scholar at the Department of Electrical Engineering and Computer Sciences of University of California, Berkeley, CA, USA, in 2010–12. Now he is the Chief Scientist and the acting Chief Technology Officer at Fano Labs, and a honorary assistant professor at the Department of Electrical and Electronic Engineering of HKU. He is a Croucher research fellow. His research interests include optimization theory and algorithms, evolutionary computation, smart grid, and smart city.